Temperature effects on the perturber induced shift of dopant ionization energies in He and Ne

C. M. Evans [a,*], Yevgeniy Lushtak [a], Xianbo Shi [b], Luxi Li [a], and G. L. Findley [c]

[a] *Department of Chemistry and Biochemistry, Queens College – CUNY, Flushing, NY 11367 and Department of Chemistry, Graduate Center – CUNY, New York, NY 10016*

[b] *NSLS II, Brookhaven National Laboratory, Upton, NY 11973*

[c] *Department of Chemistry, University of Louisiana at Monroe, Monroe, LA 71209, United States*

Abstract

In this Letter, temperature effects on the perturber induced shift $\Delta_{\mathrm{D}}(\rho_{\mathrm{P}})$ [$\rho_{\mathrm{P}} \equiv$ perturber number density] of the dopant ionization energy in the repulsive gases Ne and He are investigated at low to medium perturber number densities (i.e., $\rho_{\mathrm{P}} \leq 6.0 \times 10^{21}$ cm^{-3}). We show that these effects arise from changes in the ensemble averaged dopant/perturber polarization energy rather than from changes in the energy of the quasi-free electron.

Key words: local Wigner-Seitz model, temperature effects, dopant field ionization, quasi-free electron energy

PACS: 33.15.Ry, 34.30.+h, 31.70.-f, 31.70.Dk

1 Introduction

We have investigated the energy $V_0(\rho_{\rm P})$ [$\rho_{\rm P} \equiv$ perturber number density] of the bottom of the conduction band in a variety of atomic [1–8] and molecular perturbers [9] from low perturber number density to the density of the triple point liquid at various temperatures, including the critical temperature of the perturber. In these studies, $V_0(\rho_{\rm P})$, which is the minimum of the quasi-free electron energy, was extracted from the perturber induced shift $\Delta_{\rm D}(\rho_{\rm P})$ of the ionization energy of a dopant molecule solvated in the perturber gas, using [1,8,9]

$$V_0(\rho_{\rm P}) = \Delta_{\rm D}(\rho_{\rm P}) - P_+(\rho_{\rm P}) \ , \tag{1}$$

where $P_+(\rho_{\rm P})$ is the ensemble averaged dopant cation core/perturber energy calculated from

$$P_+(\rho_{\rm P}) = -4\pi\rho_{\rm P} \int_0^\infty g_{\rm PD}(r)\ w_+(r)\ r^2\ dr \ . \tag{2}$$

In eq. (2), $g_{\rm PD}(r)$ is the dopant/perturber radial distribution function and $w_+(r)$ is the dopant cation/perturber interaction potential. These studies [1,3–8] showed that $V_0(\rho_{\rm P})$ was independent of temperature, except near the critical density along the critical isotherm of the perturber. This critical point effect led to the development of the local Wigner-Seitz model for $V_0(\rho_{\rm P})$. However, the effects of temperature on $\Delta_{\rm D}(\rho_{\rm P})$ were probed only briefly when the local Wigner-Seitz model was extended to low density [2] for the perturbers Ar and Kr. Morever, the effect of dopant/perturber interactions on $\Delta_{\rm D}(\rho_{\rm P})$ have not been investigated in detail.

* Corresponding author.
Email addresses: cherice.evans@qc.cuny.edu (C. M. Evans),
findley@ulm.edu (G. L. Findley).

In this Letter, we present the perturber induced shift $\Delta_{\rm D}(\rho_{\rm P})$ of the dopant ionization energy, measured using field ionization of high-n dopant Rydberg states of CH_3I, NO and O_2, in the low to medium density regime (i.e., $\rho_{\rm P} \leq 6 \times 10^{21}$ cm^{-3}) for the perturbers He and Ne. These data show that the overall shift $\Delta_{\rm D}(\rho_{\rm P})$, as well as the temperature dependence of this shift, varies significantly with the dopant/perturber system in question. We then use the local Wigner-Seitz model to show that $V_0(\rho_{\rm P})$ is independent of temperature and dopant, thereby illustrating that the changes in $\Delta_{\rm D}(\rho_{\rm P})$ as a function of dopant and temperature are caused solely by changes in $P_+(\rho_{\rm P})$.

2 Experimental

The perturbers He (Matheson Gas Products, 99.9999%) and Ne (Matheson Gas Products, 99.9995% for the dopant CH_3I; AirGas, 99.999% for the dopants NO and O_2), and the dopants CH_3I (Aldrich, 99.5%), NO (Matheson Gas Products, 99.95%) and O_2 (Matheson Gas Products, 99.998%) were used without further purification. The lack of impurity interference in all dopants and perturbers was verified by both transmission and photoionization spectrometry. Prior to the introduction of a dopant/perturber system, the gas handling system [10] was baked to a base pressure of low 10^{-8} Torr; after adding a dopant, the gas handling system was allowed to return to the low 10^{-7} Torr range prior to the introduction of the perturber. The dopant concentration was maintained at < 10 ppm for all studies presented here.

As in our previous investigations [1–9], dopant photoionization spectra in Ne and in He were measured with monochromatic synchrotron radiation having a resolution of 9 meV in the spectral region of interest. The copper sample

cell is equipped with entrance and exit MgF_2 (or LiF) windows and a pair of parallel plate electrodes (stainless steel, 3.0 mm spacing) oriented parallel to the incoming radiation and perpendicular to the windows. The temperature of the cell was maintained to ± 0.5 K using an open flow cryostat and resistive heater attached to the sample cell. This cryostat is capable of cooling with either liquid N_2, used for $T > 77$ K, or liquid He (for $T < 77$ K). To prevent solidification of CH_3I and NO, all photoionization spectra of these dopants were acquired at temperatures above 173 K and 93 K, respectively. In order to measure $\Delta_D(\rho_P)$ for O_2, LiF windows were used in the sample cell, and the energy cut-off of the window was shifted by obtaining all data at temperatures below 73 K.

3 Results and Discussion

The field ionization spectra of CH_3I, NO and O_2 were obtained by taking the difference between two photoionization spectra measured with different applied electric fields (after intensity normalizing the spectra to remove the effects of secondary ionization [11]). This difference yields a peak which represents those Rydberg states ionized by the high electric field F_H but not by the low field F_L. Both F_L and F_H were optimized to produce the best field ionization signal for each dopant at each perturber number density. The time scale required for electron localization [12] in the high electric fields (i.e., between 1,000 and 10,000 V/cm) used in this study is significantly longer than that for the dopant photoionization process. Therefore, electron localization in He and in Ne does not occur during these measurements (as evidenced by the lack of change in the overall shape of the photoionization and field ionization spectra

as a function of field strength).

The perturber induced energy shift $\Delta_{\rm D}(\rho_{\rm P})$ in the dopant ionization energy is given by [1, 11]

$$\Delta_{\rm D} = I_F(\rho_{\rm P}) \; + \; c_D \, (F_L^{1/2} \; + \; F_H^{1/2}) \; - \; I_g \; , \tag{3}$$

where $I_F(\rho_{\rm P})$ is the energy of the maximum in the field ionization signal at the perturber density $\rho_{\rm P}$, c_D is the dopant-dependent field ionization constant, and I_g is the gas phase dopant ionization energy. Both c_D and I_g have been empirically determined by us from field ionization studies of the neat dopant at various electric field strengths. $I_g = 9.538 \pm 0.005$ eV and $c_{\rm CH_3I} = 4.3 \pm 0.1 \times 10^{-4}$ eV cm$^{1/2}$ V$^{-1/2}$ for CH_3I [1], while $I_g = 12.065 \pm 0.005$ eV and $c_{\rm O_2} = 4.2 \pm 0.7 \times 10^{-4}$ eV cm$^{1/2}$ V$^{-1/2}$ for O_2 [8]. For the NO data presented here, $I_g = 9.254 \pm 0.003$ eV and $c_{\rm NO} = 3.0 \pm 0.2 \times 10^{-4}$ eV cm$^{1/2}$ V$^{-1/2}$. The total error for $\Delta_{\rm D}(\rho_{\rm P})$ for all dopant/perturber systems is between 8 and 10 meV, where this error is the sum of the field correction error, the goodness-of-fit error (for fitting a field ionization spectrum to a Gaussian line shape), and the error arising from the energy uncertainty due to the resolution of the monochromator (i.e., ± 5 meV).

Figs. 1 and 2 show $\Delta_{\rm D}(\rho_{\rm P})$, measured at various temperatures, plotted as a function of reduced He and Ne number density ρ_r, respectively, for the dopants CH_3I, NO and O_2. (The reduced number density is given by $\rho_r \equiv \rho_{\rm P}/\rho_c$, where the critical density is $\rho_c = 10.5 \times 10^{21}$ cm^{-3} for He [13] and $\rho_c = 14.4 \times 10^{21}$ cm^{-3} for Ne [14].) Clearly, $\Delta_{\rm D}(\rho_{\rm P})$ is significantly different for the various dopant/perturber systems. For example, the He induced shift in the dopant ionization energy is to higher energies, while that induced by Ne is primarily toward lower energies. Similarly, $\Delta_{\rm D}(\rho_{\rm P})$ for both CH_3I and NO in Ne shifts

towards lower energies as a function of Ne density, while that for O_2 first blue shifts before red shifting. In He, lower temperatures lead to an increase in the blue shift of $\Delta_{\rm D}(\rho_{\rm P})$, while in Ne the red shift in $\Delta_{\rm D}(\rho_{\rm P})$ decreases as a function of decreasing temperature. To understand these differences requires an investigation of $P_+(\rho_{\rm P})$ as well as $V_0(\rho_{\rm P})$.

$P_+(\rho_{\rm P})$, calculated from eq. (2) with the interaction potential [1,2]

$$w_+(r) \;=\; -\,\frac{1}{2}\,\alpha\,e^2\,\sum_i^N\,r_i^{-4}\,f_+(r_i)\;, \tag{4}$$

is shown in Fig. 3 for He and in Fig. 4 for Ne. In eq. (4), α is the polarizability of the perturber, e is the electron charge, r_i is the position of each of the N perturbers relative to the dopant at the moment of ionization, and $f_+(r)$ is a screening function that incorporates the repulsive interactions between the induced dipoles in the perturbing medium. This screening function is [1,2,15]

$$\begin{aligned} f_+(r) = 1 - \alpha\,\pi\,\rho_{\rm P}\,\int_0^\infty ds\,\frac{1}{s^2}\,g_{\rm PP}(s) \\ \times\,\int_{|r-s|}^{r+s}\,dt\,\frac{1}{t^2}\,f_+(t)\,g_{\rm PD}(t)\,\theta(r,s,t)\;, \end{aligned} \tag{5}$$

where

$$\theta(r,s,t) = \frac{3}{2s^2}(s^2+t^2-r^2)(s^2-t^2+r^2) + (r^2+t^2-s^2)\;,$$

and where the integration variables s and t represent the distance between atoms of interest and all other perturber atoms. In eqs. (4) and (5), $g_{\rm PP}$ is the perturber/perturber radial distribution function, and $g_{\rm PD}$ is again the dopant/perturber radial distribution function. Thus, $P_+(\rho_{\rm P})$ is extremely sensitive to local density changes, since the local density ρ_{loc} around the dopant cation core is given by $\rho_{loc} = g_{\rm PD}(r)\rho_{\rm P}$ [16,17]. For the calculations shown in Figs. 3 and 4, the radial distribution functions $g_{\rm PD}(r)$ and $g_{\rm PP}(r)$ are determined using a coupled Percus-Yevick model [1,18] with Lennard-Jones 6-12

potentials for all dopant/perturber and perturber/perturber interactions. The Lennard-Jones parameters for these calculations are given in Table 1. Clearly, $P_+(\rho_{\rm P})$ shows a small temperature effect, which will be discussed in more detail below.

The quasi-free electron energy $V_0(\rho_{\rm P})$ is extracted from the experimental data using eq. (1), the results of which are shown in Fig. 5a for He and Fig. 5b for Ne. Fig. 5a also presents results obtained from photoinjection studies [22], for comparison. The data extracted from $\Delta_{\rm D}(\rho_{\rm P})$ obviously have lower scatter than those obtained from the photoinjection measurements. Moreover, $V_0(\rho_{\rm P})$ from the photoinjection studies is negative at low He densities, while the current data are positive at all densities. Asaf *et al.* [22] indicated that the negative $V_0(\rho_{\rm P})$ at low He densities was probably the result of surface contamination of the photocathode and, therefore, that these values did not represent a true measurement of $V_0(\rho_{\rm P})$. In the medium density range for He, $V_0(\rho_{\rm P})$ obtained from photoinjection studies do agree with those extracted here from $\Delta_{\rm D}(\rho_{\rm P})$. Fig. 5 illustrates clearly that $V_0(\rho_{\rm P})$ does not exhibit any temperature dependence, nor does it depend on the dopant. The lack of a temperature effect is consistent with the recent work on $V_0(\rho_{\rm P})$ in high density Ne [8], where the only temperature dependence was observed near the Ne critical point.

These recent Ne results [8] also confirmed that the local Wigner-Seitz model [1, 2, 9] is applicable to repulsive fluids. In this model, the quasi-free electron energy $V_0(\rho_{\rm P})$ is specified by

$$V_0(\rho_{\rm P}) \;=\; P_-(\rho_{\rm P}) \;+\; E_k(\rho_{\rm P}) \;+\; \frac{3}{2}\, k_B\, T \;, \tag{6}$$

where $(3/2\ k_BT)$ is the thermal energy of the quasi-free electron. The ensemble averaged electron/perturber polarization energy $P_-(\rho_{\rm P})$ in eq. (6) is

determined from [1, 9, 15]

$$P_{-}(\rho_{\rm P}) \;=\; -\,4\,\pi\,\rho_{\rm P}\,\int_0^\infty g_{\rm PP}(r)\;w_{-}(r)\;r^2\;dr\;, \tag{7}$$

and the zero point kinetic energy $E_k(\rho_{\rm P})$ of the quasi-free electron is calculated using [8, 9]

$$E_k(\rho_{\rm P}) \;=\; \frac{\hbar^2\;\eta_0^2}{2\,m_e\;(r_\ell\;-\;|A|)^2}\;. \tag{8}$$

In eqs. (7) and (8), $w_{-}(r)$ is the electron/perturber interaction potential, r_ℓ is the local Wigner-Seitz radius (i.e., $r_\ell = \sqrt[3]{3/(4\pi g_m \rho_{\rm P})}$, where g_m is the maximum of $g_{\rm PP}$), A is the zero kinetic energy electron scattering length, and η_0 is a phase shift induced by the short-ranged electron/perturber interaction potential. The solid line in Fig. 5b shows the local Wigner-Seitz calculation for $V_0(\rho_{\rm P})$ in Ne. This result, which was published previously [8], was obtained with $A = 0.10$ Å and $\eta_0 = 0.65$ and with $g_{\rm PP}(r)$ determined using the Ne/Ne parameters given in Table 1. The solid line in Fig. 5a represents a local Wigner-Seitz calculation for He for the low to medium perturber number densities presented here. For this model, $A = 0.57$ Å [23] and $g_{\rm PP}(r)$ was calculated using the He/He parameters given in Table 1. The phase shift $\eta_0 = 0.78$ was adjusted to give the best results for the extracted $V_0(\rho_{\rm P})$ as well as for the average value 1.0 ± 0.3 eV for $V_0(\rho_{\rm P})$ [24] at the liquid density 22×10^{21} cm^{-3}. Clearly, the local Wigner-Seitz model fits $V_0(\rho_{\rm P})$ for He as well as for Ne [8]. As with Ne, the strictly positive nature of $V_0(\rho_{\rm P})$ in He is caused by the domination of the zero-point kinetic energy $E_k(\rho_{\rm P})$ over the ensemble averaged electron/He polarization energy $P_{-}(\rho_{\rm P})$. (A more detailed investigation of the local Wigner-Seitz model in He will require experimental data with minimal scatter at higher densities as well as data obtained near the critical point. These studies are currently in progress by us.)

Since $V_0(\rho_P)$ is independent of temperature (except at the critical temperature) and dopant, the effects of temperature and dopant on $\Delta_D(\rho_P)$, observed in Figs. 1 and 2, are caused by changes in $P_+(\rho_P)$. In both He (cf. Fig. 3) and Ne (cf. Fig. 4), the red shift in $P_+(\rho_P)$ decreases as a function of decreasing temperature, with the decrease being more pronounced in He. Moreover, this behavior contrasts sharply with that of CH_3I in Ar [2], where the red shift in $P_+(\rho_P)$ increases with decreasing temperature. In Ar, the maximum in the dopant/perturber radial distribution function $g_{PD}(r)$ increases as the temperature decreases, thereby leading to an increase in the red shift of $P_+(\rho_P)$. In Ne and He, on the other hand, the maximum in $g_{PD}(r)$ decreases as the temperature decreases, resulting in a decrease in the red shift of $P_+(\rho_P)$. Thus, the increasing blue shift in $\Delta_D(\rho_P)$ in He (cf. Fig. 1), as well as the decreasing red shift in $\Delta_D(\rho_P)$ in Ne (cf. Fig. 2), can be explained by the decrease in the perturber dependent energy shift in $P_+(\rho_P)$ as a function of decreasing temperature when coupled with the strictly positive $V_0(\rho_P)$.

$\Delta_D(\rho_P)$ for O_2/Ne (cf. Fig. 4c) is strikingly different than that for CH_3I/Ne and NO/Ne. This difference results from the competition between the red-shifting $P_+(\rho_P)$ and the blue shifting $V_0(\rho_P)$ as a function of Ne number density. At low Ne densities (i.e., $\rho_r < 0.1$), $V_0(\rho_P)$ dominates, leading to the blue shift in $\Delta_D(\rho_P)$. As the density increases, $P_+(\rho_P)$ becomes the dominant term in eq. (1), resulting in the red shift observed for $\rho_r > 0.1$.

The original low density model developed by Fermi [26, 28], as modified by Alekseev and Sobel'man [27, 28], assumed that dopant/perturber interactions are negligible at low perturber number densities. Therefore, in that model $\Delta_D(\rho_P)$ is identical for all dopants solvated in the same perturber, which is clearly contradicted by Figs. 1 and 2. Moreover, the temperature dependence

in $P_+(\rho_P)$ arises solely from the change in the average velocity of the perturber molecules [26–28], resulting in a red shift in $P_+(\rho_P)$ that always decreases with decreasing temperature. However, previous results of CH_3I in Ar [2] have shown that the red shift in $P_+(\rho_P)$ can increase as a function of decreasing temperature. From the current results of $\Delta_D(\rho_P)$ in low density Ne and He coupled to the previous results in Ar [2], one can conclude that the original low density model [26–28] for $P_+(\rho_P)$ fails in the low to medium density regime.

4 Conclusion

In this Letter, we have presented the perturber induced shift $\Delta_D(\rho_P)$ of dopant ionization energies for various dopants in both Ne and He at low to medium perturber number densities. We showed that the observed dopant and temperature dependencies in $\Delta_D(\rho_P)$ arise from differences in the ensemble averaged dopant cation/perturber polarization energy $P_+(\rho_P)$. We used $\Delta_D(\rho_P)$ to extract $V_0(\rho_P)$ in He at low to medium number densities with minimal scatter, and subsequently showed that $V_0(\rho_P)$ in He can be interpreted within the local Wigner-Seitz model.

5 Acknowledgement

The experimental measurements reported here were performed at the University of Wisconsin Synchrotron Radiation Center (NSF DMR-0537588). This work was supported by grants from the Petroleum Research Fund (45728-B6), from the Louisiana Board of Regents Support fund (LEQSF (1997-00)-RD-A-14), from the Professional Staff Congress–City University of New York (62386-

00 40), and from the National Science Foundation (NSF CHE-0956719).

References

[1] C. M. Evans, G. L. Findley, Phys. Rev. A 72 (2005) 022717.

[2] Xianbo Shi, Luxi Li, Gina M. Moriarty, C. M. Evans, G. L. Findley, Chem. Phys. Lett. 454 (2008) 12.

[3] C. M. Evans, G. L. Findley, Chem. Phys. Lett. 410 (2005) 242.

[4] C. M. Evans, G. L. Findley, J. Phys. B: At. Mol. Opt. Phys. 38 (2005) L269.

[5] Luxi Li, C. M. Evans, G. L. Findley, J. Phys. Chem. A 109 (2005) 10683.

[6] Xianbo Shi, Luxi Li, C. M. Evans, G. L. Findley, Chem. Phys. Lett. 432 (2006) 62.

[7] Xianbo Shi, Luxi Li, C. M. Evans, G. L. Findley, Nucl. Inst. Meth. Phys. A 582 (2007) 270.

[8] C. M. Evans, Yevgeniy Lushtak, G. L. Findley, Chem. Phys. Lett. 501 (2011) 202.

[9] Xianbo Shi, Luxi Li, G. L. Findley, C. M. Evans, Chem. Phys. Lett. 481 (2009) 183.

[10] C. M. Evans, J. D. Scott, G. L. Findley, Recent Res. Dev. Chem. Phys. 3 (2002) 351.

[11] A. K. Al-Omari, Ph.D. dissertation, University of Wisconsin Madison, Madison, WI, 1996, and references therein.

[12] M. Rosenblit, J. Jortner, J. Phys. Chem. A 101, 751 (1997).

[13] R. D. McCarty, J. Phys. Chem. Ref. Data 2 (1973) 923.

[14] R. D. McCarty, R. B. Stewart, in S. Gratch (Eds.), Advances in Thermophysical Properties at Extreme Temperatures and Pressures, American Society of Mechanical Engineers, New York, 1965, p. 84.

[15] J. Lekner, Phys. Rev. 158 (1967) 130.

[16] P. Attard, J. Chem. Phys. 91 (1989) 3072.

[17] P. Attard, J. Chem. Phys. 91 (1989) 3083.

[18] E. W. Grundke, D. Henderson, R. D. Murphy, Can. J. Phys. 48 (1968) 2720.

[19] N. M. Putintsev, D. N. Putintsev, Doklady Phys. Chem. 399 (278) 2004.

[20] F. M. Mourits, F. H. A. Rummens, Can. J. Phys. 51 (1977) 3007.

[21] P. T. Sikora, J. Phys. B: At. Mol. Opt. Phys. 3 (1970) 1475.

[22] U. Asaf, I. T. Steinberger, Chem. Phys. Lett. 128 (1986) 91.

[23] A. M. Köhler, V. Saile, R. Reininger, G. L. Findley, Phys. Rev. Lett. 60 (1988) 2727.

[24] J. R. Broomall, W. D. Johnson, D. G. Onn, Phys. Rev. B 14 (1976) 2819, and references therein.

[25] R. H. Orcutt, R. H. Cole, J. Chem. Phys. 46 (1967) 697.

[26] E. Fermi, Nuovo Cimento 11 (1934) 157.

[27] V. A. Alekseev, I. I. Sobel'man, Sov. Phys. JETP 22 (1966) 882.

[28] A. M. Köhler, R. Reininger, V. Saile, G. L. Findley, Phys. Rev. A 33 (1986) R771.

Table 1
Lennard-Jones parameters used in the calculation of $g_{\mathrm{PD}}(r)$ and $g_{\mathrm{PP}}(r)$.

	σ Å	ε/k_B (K)	Ref.
He–He	2.576	10.2	[19]
CH_3I–He	3.763	12.9	a
NO–He	3.218	15.0	a
O_2–He	3.174	15.3	a
Ne–Ne	2.782	37.3	[20]
CH_3I–Ne	3.763	47.2	a
NO–Ne	3.065	50.7	a
O_2–Ne	3.028	50.5	a

[a]Determined from the Sikora combining rules [21], with small (i.e., $< 1\%$) adjustments being made to obtain the best fit to experiment.

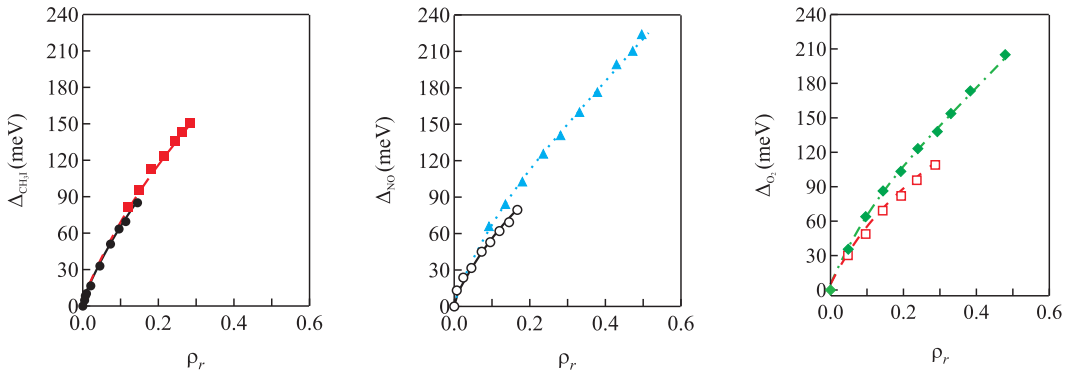

Fig. 1. [Color online] He induced shift $\Delta_{\rm D}(\rho_{\rm P})$ of the dopant ionization energy plotted as a function of reduced He number density $\rho_r \equiv \rho_{\rm P}/\rho_c$ at various temperatures. (The critical density for He is $\rho_c = 10.5 \times 10^{21}$ cm^{-3} [13].) D = CH_3I, NO and O_2. Temperatures are (●,○) 298 K, (■,□) 173 K, (▲) 93 K, and (♦) 73 K. The lines result from eq. (1) with $P_+(\rho_{\rm P})$ calculated from eq. (2) and $V_0(\rho_{\rm P})$ determined from eq. (6), as discussed below. The average total experimental error is ∼ 9 meV for all data points shown.

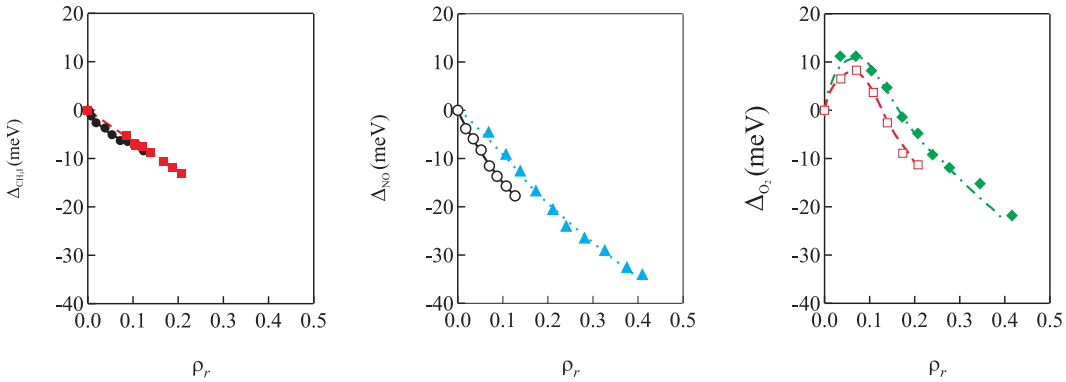

Fig. 2. [Color online] Ne induced shift $\Delta_{\rm D}(\rho_{\rm P})$ of the dopant ionization energy plotted as a function of reduced Ne number density $\rho_r \equiv \rho_{\rm P}/\rho_c$ at various temperatures. (The critical density for Ne is $\rho_c = 14.5 \times 10^{21}$ cm^{-3} [14].) D = CH_3I, NO, and O_2. Temperatures are (●,○) 298 K, (■,□) 173 K, (▲) 93 K, and (♦) 73 K. The lines result from eq. (1) with $P_+(\rho_{\rm P})$ calculated from eq. (2) and $V_0(\rho_{\rm P})$ determined from eq. (6), as discussed below. The average total experimental error is ∼ 9 meV for all data points shown.

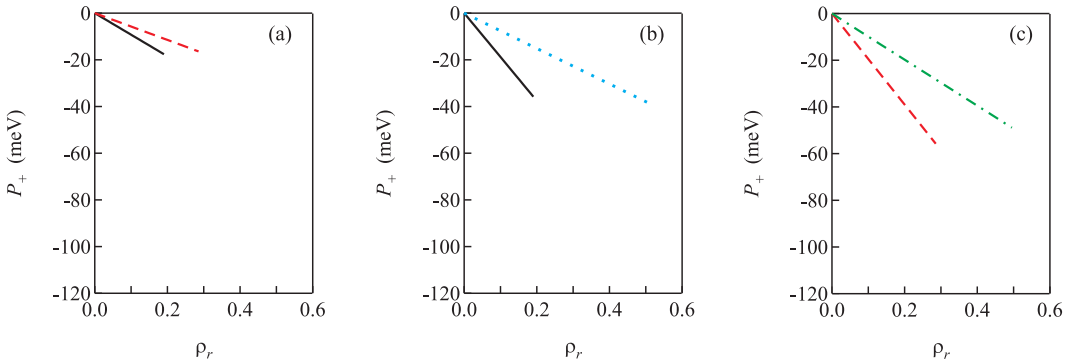

Fig. 3. [Color online] $P_+(\rho_P)$ calculated from eq. (2) for (a) CH_3I, (b) NO, and (c) O_2 in He plotted as a function of reduced He number density $\rho_r \equiv \rho_P/\rho_c$ at various temperatures. (—) 298 K, (– –) 173 K, (· · ·) 93 K, and (– · –) 73 K.

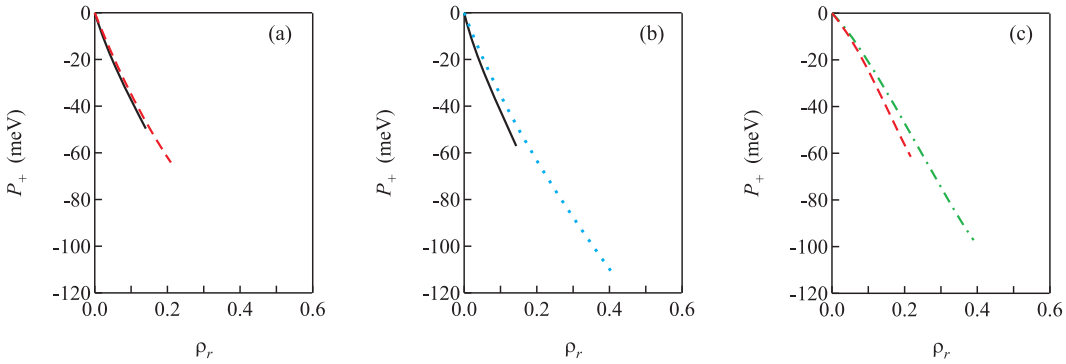

Fig. 4. [Color online] $P_+(\rho_P)$ calculated from eq. (2) for (a) CH_3I, (b) NO, and (c) O_2 in Ne plotted as a function of reduced Ne number density $\rho_r \equiv \rho_P/\rho_c$ at various temperatures. (—) 298 K, (– –) 173 K, (· · ·) 93 K, and (– · –) 73 K.

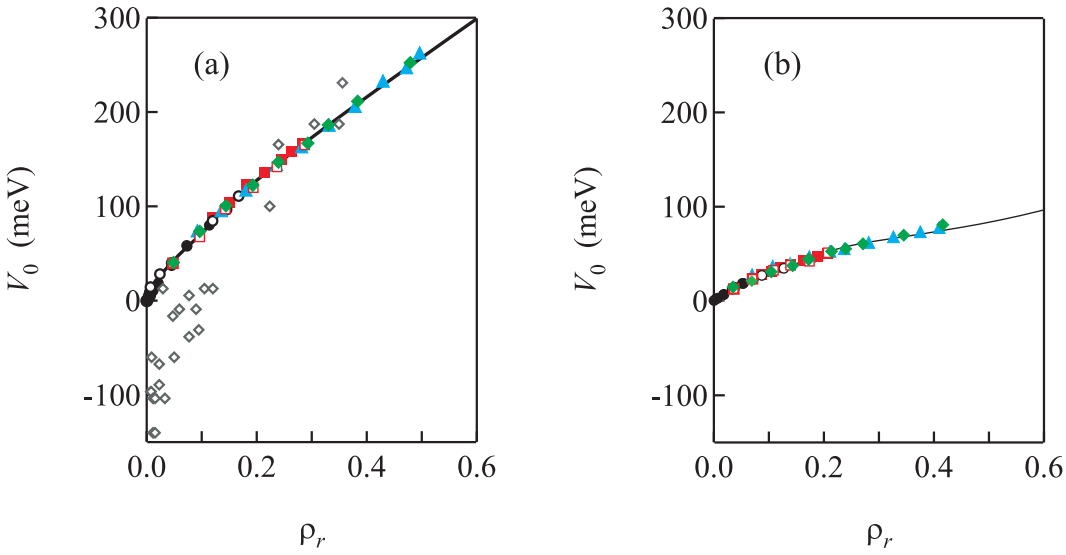

Fig. 5. [Color online] The minimum energy $V_0(\rho_P)$ of the (a) He and (b) Ne conduction band plotted as a function of reduced perturber number density ρ_r. (●,○) 298 K, (■,□) 173 K, (▲) 93 K, and (♦) 73 K. (●,■) D = CH_3I, (○,▲) D = NO, and (□,♦) D = O_2. (◊) are previous low density results obtained from photoinjection measurements [22]. The lines are local Wigner-Seitz calculations of $V_0(\rho_P)$: details of which are given in the text; details of the Ne calculation are given in [8].